Clustering of floating tracers in weakly divergent velocity fields

Konstantin V. Koshel[*] and Dmitry V. Stepanov[†]

V.I. Il'ichev Pacific Oceanological Institute, FEB RAS, Vladivostok 690041, Russia

Eugene A. Ryzhov[‡] and Pavel Berloff[§]

Department of Mathematics, Imperial College London, London SW7 2AZ, United Kingdom

V. I. Klyatskin[‖]

A.M. Obukhov Atmospheric Physics Institute, RAS, Moscow 119017, Russia

This work deals with buoyant tracers floating at the ocean surface, where the geostrophic velocity component is two dimensional and rotational (nondivergent) and the ageostrophic component can contain rotational and potential (divergent) contributions that are comparable in size. We consider a random kinematic flow model and study the process of clustering, that is, aggregation of the floating tracer in localized spatial patches. In the long-time limit and in the cases of strongly and weakly divergent flows, the existing analytical theory predicts the process of exponential clustering, which is the emergence of spatial singularities containing all the available tracer. Here we confirm this analytical prediction, in numerical model solutions spanning different combinations of rotational and potential surface velocity components, and report that exponential clustering persists even in weakly divergent flows, however at significantly slower rates. For a wide range of parameters, we analyze not only the exponential clustering but also the other type of tracer aggregation, referred to as fragmentation clustering, as well as the coarse-graining effects on clustering. For the presented analysis we consider ensembles of Lagrangian particles and introduce and apply the statistical topography methodology.

I. INTRODUCTION

In turbulent oceanic and atmospheric flows, the phenomenon of clustering, i.e., spatial aggregation of various tracers and objects, manifests itself in different physical situations and on different spatial scales [1–3]. More generally, clustering processes are studied in marine ecosystems [1], the formation of clouds [4], porous media [5], palaeontology [6], cosmology [7], etc. Most relevant to our study are clusterings of floating debris and plastic litter, e.g., in garbage islands [8,9], and of oil spills and sargassum [3]. These actively researched problems are practically important, because of the environmental concerns due to the ocean pollution, in general, and due to the adverse effect of positive correlations between aggregations of pollution and marine life.

Our focus is on clustering of floating tracers at the ocean surface [10–19]. Since this process is largely driven by the multiscale and transient surface velocity, we are motivated by the systematic theoretical study of the clustering in random, progressively more complicated and realistic kinematic velocity fields and further in dynamically constrained flows.

At the ocean surface within the mesoscale range, the dominant, i.e., leading-order, geostrophic velocity can be treated as nondivergent (hence purely rotational). The small ageostrophic first-order corrections are three-dimensional (3D) motions; hence they are 2D divergent at the surface [20–25] and can be treated as a combination of divergent (potential) and rotational (nondivergent) components. The latter is largely responsible for the clustering process [11,26–37].

Some asymptotic theories of clustering, including for the weakly divergent velocities, have been developed for random and turbulent kinematic flows [10,11,31,35,36,38–43], but the actual transitions towards the predicted asymptotic behaviors remain poorly understood [18], despite their obvious relevance for real geophysical phenomena. The main goal of this paper is to establish statistical properties of clustering in random kinematic flows, before the asymptotic states are clearly reached, and in the Monte Carlo sense for ensembles of Lagrangian particles.

The paper is organized in the following way. Section II formulates the problem and outlines the mathematical foundations of the statistical topography to be used. Section III considers both the kinematic flow model and the numerical implementation of the clustering analysis. The main results are given in Sec. IV. A summary and discussion are in Sec. V.

II. PROBLEM FORMULATION

The tracer evolution dynamics at the ocean surface can be formulated for both passive and floating tracers and the corresponding dynamical descriptions fundamentally differ, thus reflecting profoundly different clustering properties. Understanding these differences is an essential part of the general

---

[*]kvkoshel@poi.dvo.ru

[†]step-nov@poi.dvo.ru

[‡]Also at V.I. Il'ichev Pacific Oceanological Institute, FEB RAS, Vladivostok 690041, Russia; ryzhovea@gmail.com
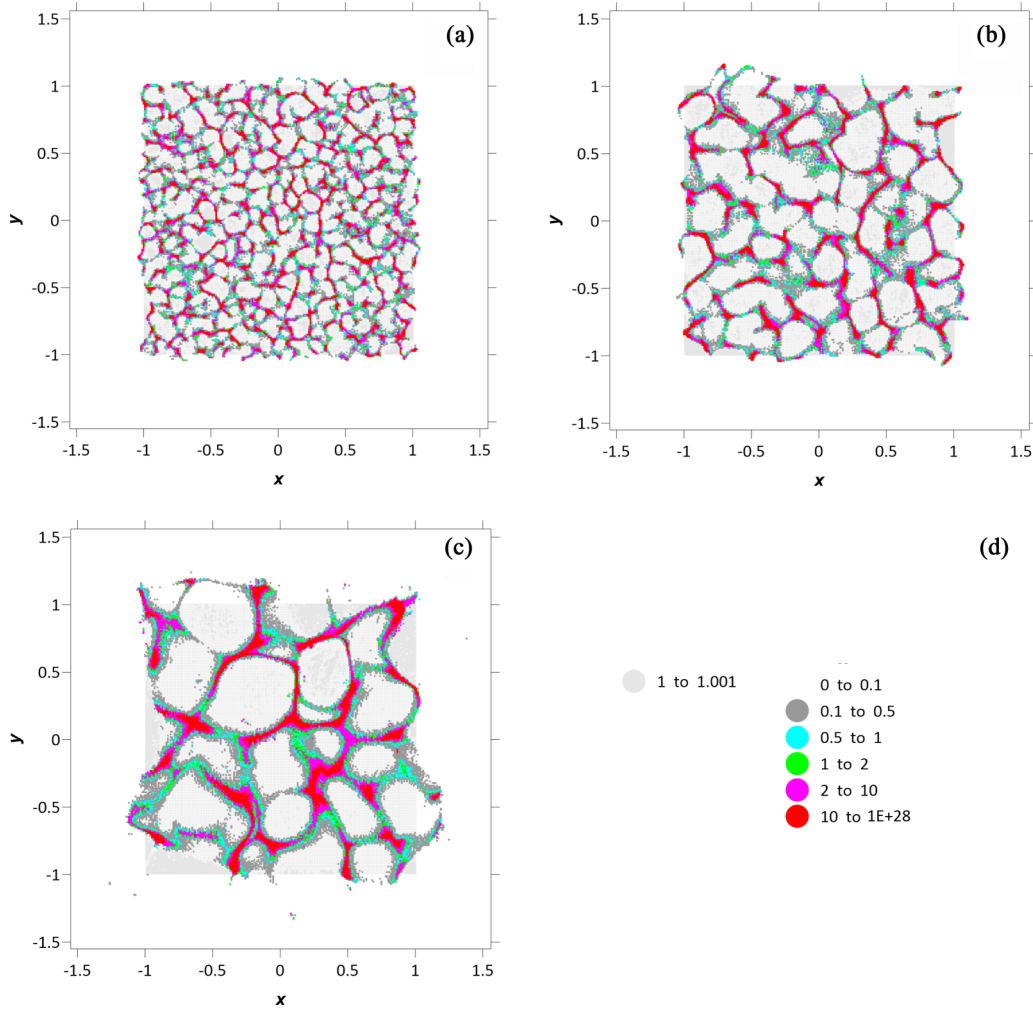
[§]p.berloff@imperial.ac.uk

[‖]klyatskin@yandex.ru

FIG. 1. Density distributions for the purely divergent velocity regime ($\gamma = 1$) for $t = \tau$ and (a) $l = 0.04$ and $\sigma_U = 0.33$, (b) $l = 0.08$ and $\sigma_U = 0.33$, and (c) $l = 0.16$ and $\sigma_U = 0.67$. The gray square indicates the initial density distribution. The color scale indicates (nondimensional) values of the tracer density.

fundamental understanding of the clustering process. First, let us introduce the passive-tracer concentration $C(\mathbf{r}, t)$ and floating-tracer density $\rho(\mathbf{r}, t)$, which are the main fields of interest, both varying in space and evolving in time (here $\mathbf{r}$ is the 3D position vector and t is time), subject to a 3D velocity field $\mathbf{u}(\mathbf{r}, t)$. Second, let us discuss differences between C and ρ and explain the terminology. The passive tracer is just a marker of fluid (and fluid particles) and its dynamics is subject to the standard continuity equation for material tracers; in turn, this equation can be restricted to describe the evolution of C on the ocean surface. Since our study deals only with incompressible fluids, i.e., with 3D nondivergent velocity fields, the concentration C is also incompressible and conserved on material particles. On the other hand, the floating tracer is not passive, in the sense that it experiences the buoyancy force that keeps it floating at the surface; therefore, it is not a marker of fluid (and material particles), its dynamics is subject to the continuity equation for the floating tracer, and its density changes along fluid particle trajectories due to the surface velocity divergence. The latter effect can be viewed as compressibility of the floating-tracer density ρ, which justifies our choice of terminology: "density"

for floating (compressible) tracers versus "concentration" for passive (incompressible) tracers.

At the ocean surface, the flow velocity can be written as $\mathbf{u}(\mathbf{R}, 0, t) = (\mathbf{U}(\mathbf{R}, t), w(\mathbf{R}, 0, t))$, where $\mathbf{U}$ and w are the horizontal and vertical velocity components, respectively, and $\mathbf{R} = (x, y)$ is the 2D coordinate at the surface. The dynamical equations governing concentration C and density ρ at the ocean surface (derived in the Appendix) are

$$\left(\frac{\partial}{\partial t} + \mathbf{U}(\mathbf{R}, t) \frac{\partial}{\partial \mathbf{R}} \right) C(\mathbf{R}, t) = \kappa \Delta_{\mathbf{R}} C(\mathbf{R}, t),$$

$$C(\mathbf{R}, 0) = C_0(\mathbf{R}), \qquad (1)$$

$$\left(\frac{\partial}{\partial t} + \frac{\partial}{\partial \mathbf{R}} \mathbf{U}(\mathbf{R}, t) \right) \rho(\mathbf{R}, t) = \kappa \Delta_{\mathbf{R}} \rho(\mathbf{R}, t),$$

$$\rho(\mathbf{R}, 0) = \rho_0(\mathbf{R}), \qquad (2)$$

where $C_0(\mathbf{R})$ and $\rho_0(\mathbf{R})$ are the initial concentration and density distributions, respectively, $\Delta_{\mathbf{R}}$ is the 2D Laplacian, and κ is the diffusivity. For the sake of initial simplicity, in what follows we will consider the tracer dynamics in an unbounded domain and for the adiabatic case $\kappa = 0$ while
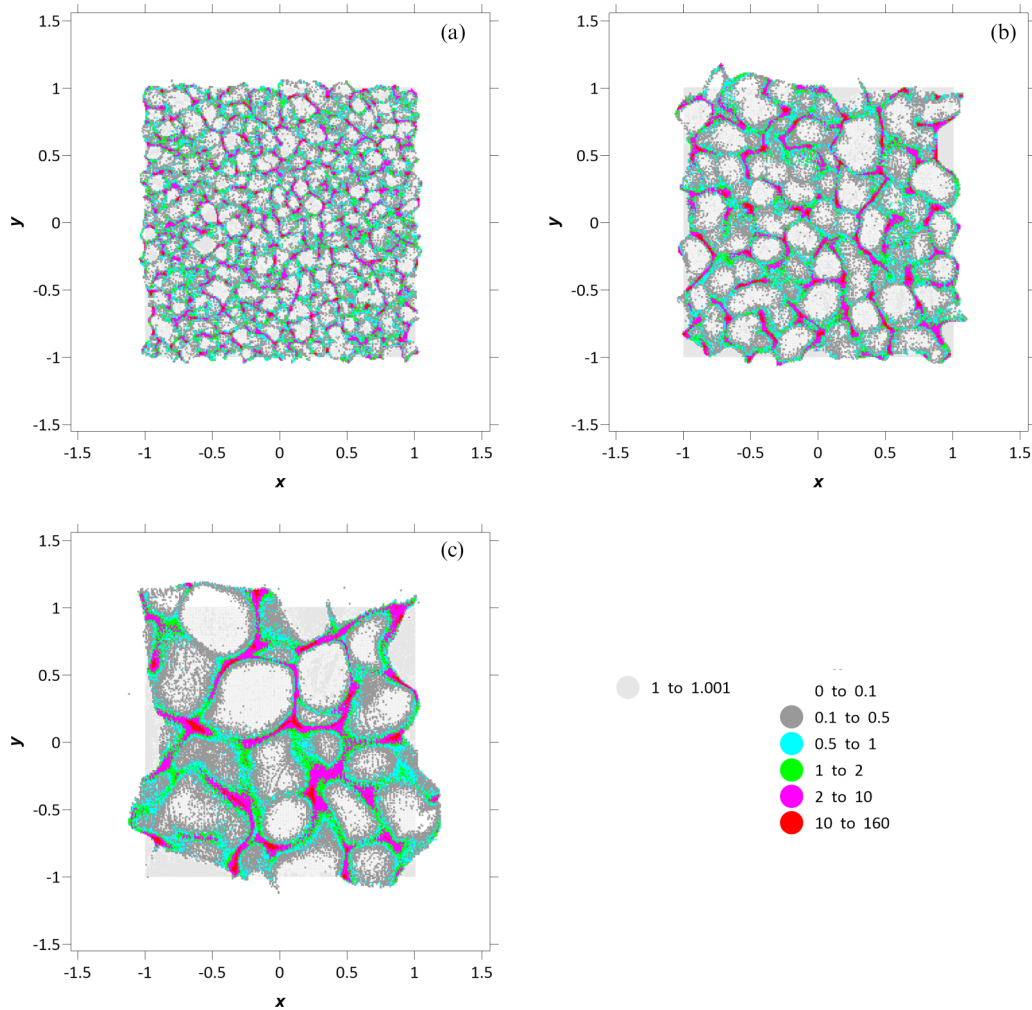
FIG. 2. Normalized number of particles for the purely divergent velocity regime ($\gamma = 1$) for $t = \tau$ and (a) $l = 0.04$ and $\sigma_U = 0.33$, (b) $l = 0.08$ and $\sigma_U = 0.33$, and (c) $l = 0.16$ and $\sigma_U = 0.67$. The gray square indicates the initial density distribution. The color scale indicates (normalized) number of particles.

recognizing that both of these factors can be important and should be studied separately.

In what follows the governing equations are nondimensionalized by the specified length scale L^*, timescale t^*, and density scale ρ^*. The time discretization step for the numerical random velocity field is taken to be the timescale $t^* = t_0$, since the random velocity is taken to be δ correlated in time. The length scale L^* is chosen so that the initial area occupied by the tracer is 4. The spatial discretization step is h_0 and the discretization steps are interdependent $h_0/t_0 = $ const; we use $h_0/t_0 = 1$. The initial density of the tracer is unity; the velocity scale is $U^* = L^*/t^*$ and the turbulent diffusion scale is $\kappa^* = (L^*)^2/t^*$.

A. Types of clustering and terminology

For the problem in hand, we discuss (though with widely different emphases) three types of surface clustering, referred to as C, D, and L clustering, with their specifics described further below.

The C-clustering process refers to the passive-tracer concentration clustering. Since in the absence of diffusion C is materially conserved, its Lagrangian values cannot change,

e.g., even when Lagrangian particles aggregate or their densities tend to infinity. Therefore, C clusters can form only as part of the fragmentation process due to nonuniform flow advection of the initially inhomogeneous distribution $C_0(x, y)$; in general, this is just an aspect of chaotic stirring [44–47]. Clearly, the adiabatic values of $C(x, y, t)$ are always bounded by the minimum and maximum values of $C_0(x, y)$. A C clustering can be described and quantified both locally and in a coarse-grained sense, i.e., by averaging over spatial bins. Considering coarse-graining effects is important, because they are often observed in geophysical applications [43]. Since we consider only floating particles here, the C clustering is not in our model, but it might be considered as the fragmentation of the tracer patch boundary.

The D-clustering process refers to the floating-tracer density clustering and is so much in the focus of our study that we also refer to it as simply the clustering process. Although D clustering is also affected by the fragmentation, more importantly, it can experience the exponential clustering process, which is the main subject of our study. Clearly, the adiabatic values of $\rho(x, y, t)$ are not bounded by the minimum and maximum values of $\rho_0(x, y)$ and can grow to infinity

over the area that shrinks to zero; this is the essence of the exponential clustering. A D clustering can be described and quantified both locally and in a coarse-grained sense, but the latter description has subtleties, which we will discuss in due course. Note that D clustering can happen even in the absence of C clustering, and the difference between them is fully due to the profound physical and dynamical differences between the passive and floating tracers, as reflected in (1) and (2).

The L-clustering process refers to the clustering of surface Lagrangian-particle ensembles, without any concern to their concentration or density values. Clearly, L clustering can happen even when there is no C clustering, e.g., when the initial concentration is homogeneous, but the surface velocity is divergent. Note that L clustering can be fundamentally described only in a coarse-grained way, as it involves averaging over many Lagrangian particles, i.e., by calculating their normalized number, and cannot be applied to a single particle. Since L clustering can be both fragmental, e.g., when the initial distribution of particles is inhomogeneous, and exponential, e.g., when all particles converge to a point, its coarse graining can be also subtle. Finally, L clustering and D clustering occur together, but their characteristics are significantly different. This distinction has profound implications: The description of a floating-tracer clustering by simply following Lagrangian particles and detecting their aggregations is a valid one, but it does not describe the corresponding floating-tracer density field and has limited information content.

B. Random velocity fields: Statistical properties

First, we decompose the random surface velocity as

$$\mathbf{U}(\mathbf{R}, t) = \gamma \mathbf{U}^p(\mathbf{R}, t) + (1 - \gamma)\mathbf{U}^s(\mathbf{R}, t), \quad (3)$$

where superscripts p and s indicate the divergent, i.e., potential and compressible, and rotational, i.e., solenoidal and nondivergent, velocity field components, respectively, and $0 \leqslant \gamma \leqslant 1$ is the nondimensional parameter setting their relative contributions. Second, we define statistical properties of the random velocity following [28,35,48]: Both $\mathbf{U}^p(\mathbf{R}, t)$ and $\mathbf{U}^s(\mathbf{R}, t)$ are δ-correlated-in-time random fields with Gaussian, spatially homogeneous, isotropic, and stationary statistics. For such random fields the spatiotemporal velocity correlation tensors are

$$B_{\alpha\beta}^j(\mathbf{R}', \eta) = \left\langle U_\alpha^j(\mathbf{R}, t) U_\beta^j(\mathbf{R} + \mathbf{R}', t + \eta) \right\rangle$$
$$= \int d\mathbf{k}\, E_{\alpha\beta}^j(\mathbf{k}, \eta) e^{i\mathbf{k}\cdot\mathbf{R}'}, \quad (4)$$

where $\boldsymbol{k} = (k_x, k_y)$ is the 2D wave vector such that $k = |\boldsymbol{k}|$; α and β stand for x and y, respectively; j stands for either p or s; $\mathbf{R}'$ is a 2D spatial shift; η is a time lag; and $\langle \cdots \rangle$ denotes ensemble averaging over many velocity field realizations. The spectral densities are

$$E_{\alpha\beta}^p(\mathbf{k}, \eta) = E^p(k, \eta)\frac{k_\alpha k_\beta}{k^2},$$
$$E_{\alpha\beta}^s(\mathbf{k}, \eta) = E^s(k, \eta)\left(\delta_{\alpha\beta} - \frac{k_\alpha k_\beta}{k^2}\right), \quad (5)$$
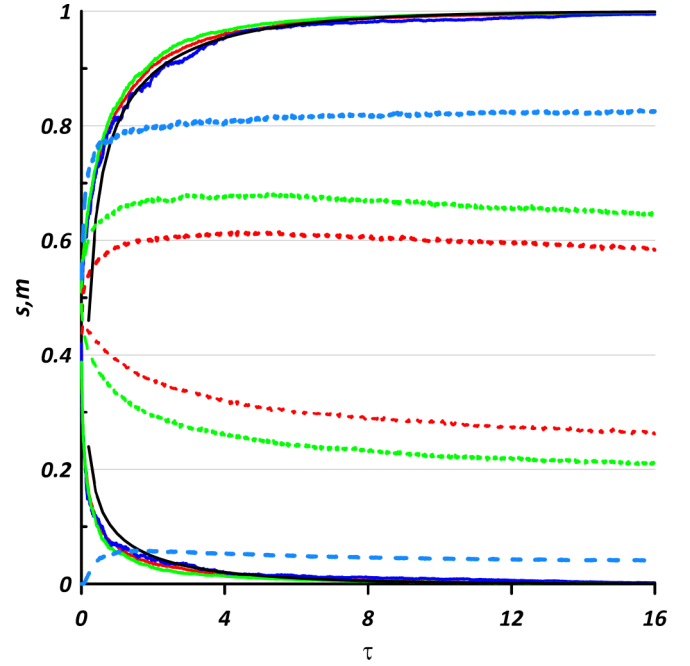

FIG. 3. Time evolution of the clustering area (decreasing curves) and mass (increasing curves) corresponding to the threshold value $\bar{\rho} = 1$ and a single velocity realization. The parameters correspond to those in Fig. 1: (a) red, (b) green, and (c) blue lines. The black lines represent the asymptotics (22). The dashed lines illustrate the corresponding solution for $\gamma = 0$ (Fig. 4).

where $\delta_{\alpha\beta}$ is the Kronecker delta. The space-time local velocity correlation tensor is

$$B_{\alpha\beta}^j(\mathbf{0}, 0) = \left\langle U_\alpha^j(\mathbf{R}, t) U_\beta^j(\mathbf{R}, t) \right\rangle = \tfrac{1}{2}\sigma_U^2 \delta_{\alpha\beta}, \quad (6)$$

where $\sigma_U^2 = B_{\alpha\alpha}(\mathbf{0}, 0) = \int d\mathbf{k}\, E(k, 0)$. Let us introduce the effective diffusivities [28,35,36]

$$D^p = \int_0^\infty d\eta \int d\mathbf{k}\, k^2 E^p(k, \eta)$$
$$= \int_0^\infty d\eta \langle [\boldsymbol{\nabla}_\mathbf{R} \cdot \mathbf{U}(\mathbf{R}, t + \eta)][\boldsymbol{\nabla}_\mathbf{R} \cdot \mathbf{U}(\mathbf{R}, t)] \rangle, \quad (7)$$

$$D^s = \int_0^\infty d\eta \int d\mathbf{k}\, k^2 E^s(k, \eta)$$
$$= \frac{1}{2}\int_0^\infty d\eta \langle [\boldsymbol{\nabla} \times \mathbf{U}(\mathbf{R}, t + \eta)] \cdot [\boldsymbol{\nabla} \times \mathbf{U}(\mathbf{R}, t)] \rangle, \quad (8)$$

where $\boldsymbol{\nabla}_\mathbf{R} \cdot \mathbf{U}(\mathbf{R}, t)$ is the velocity divergence and $\boldsymbol{\nabla} \times \mathbf{U}(\mathbf{R}, t)$ is the velocity curl. The diffusivities arise from the time-lag-integrated correlation tensor

$$B_{kl}^{\mathrm{eff}}(\mathbf{r}) = \int_0^\infty d\tau B_{kl}(\mathbf{r}, \tau), \quad B_{kl}^{\mathrm{eff}}(0) = D^0 \delta_{kl},$$

$$\frac{\partial}{\partial r_i} B_{kl}^{\mathrm{eff}}(0) = 0 \quad (9)$$

and its second derivatives

$$-8\frac{\partial^2}{\partial r_i \partial r_j} B_{kl}^{\mathrm{eff}}(0) = D^s(2\delta_{kl}\delta_{ij} - \delta_{ki}\delta_{lj} - \delta_{kj}\delta_{li})$$
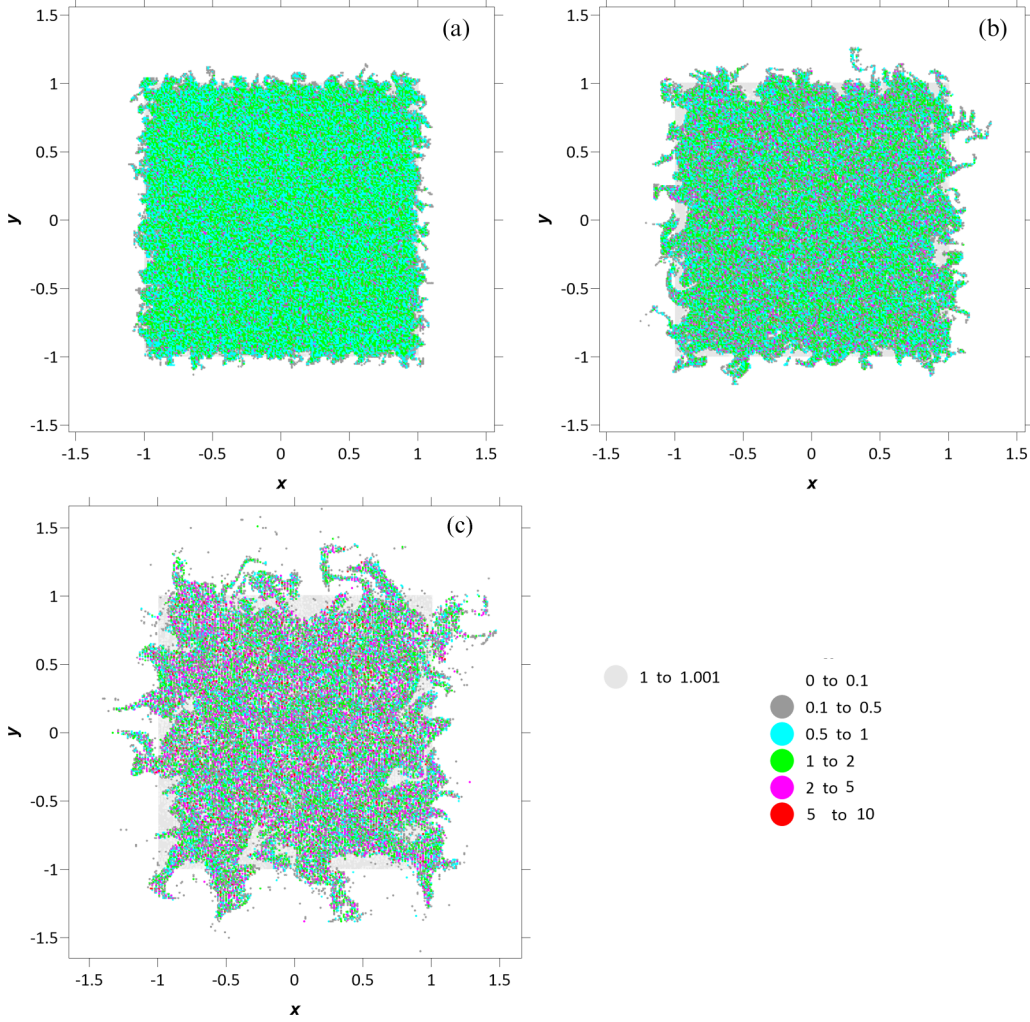$$+ D^p(2\delta_{kl}\delta_{ij} + \delta_{ki}\delta_{lj} + \delta_{kj}\delta_{li}). \quad (10)$$

FIG. 4. Density distributions for the purely rotational velocity regime ($\gamma = 0$) for $t = \tau$ and (a) $l = 0.04$ and $\sigma_U = 0.33$, (b) $l = 0.08$ and $\sigma_U = 0.33$, and (c) $l = 0.16$ and $\sigma_U = 0.67$. The gray square indicates the initial density distribution. The color scale indicates (nondimensional) values of the tracer density.

In combination with the statistical topography methodology, the diffusivities will be used in the clustering analyses of Sec. IV.

C. Statistical topography of random fields

A brief description of the statistical topography methodology, applied here for a quantitative description of the clustering process, follows [30,35]. Let the density field $\rho(\mathbf{R}, t)$ be a random in time process at a fixed point $\mathbf{R}$ with a single-point probability density function (PDF), which is homogeneous in space but evolving in time. We assume that, from the initial density distribution, the dynamics generates a population of clusters, which are localized regions with large density. A solution corresponding to the log-normal process, which describes the clustering for a purely divergent velocity field, i.e., $\gamma = 1$, has the PDF (see, e.g., [30,35])

$$P(t; \rho) = \frac{1}{2\rho\sqrt{\pi t/\tau}} \exp\left\{-\frac{\ln^2(\rho e^{t/\tau}/\rho_0)}{4t/\tau}\right\}, \quad (11)$$

where $\tau = 1/D^p$ is the effective diffusion timescale. The corresponding integral distribution function is

$$\Phi(t; \rho) \equiv \int_0^\rho d\rho' P(t; \rho') = \mathrm{Pr}\left(\frac{\ln^2(\rho e^{t/\tau}/\rho_0)}{2\sqrt{t/\tau}}\right), \quad (12)$$

where $\mathrm{Pr}(z)$ is the probability integral

$$\mathrm{Pr}(z) = \frac{1}{\sqrt{2\pi}} \int_{-\infty}^z dx \exp\left\{-\frac{x^2}{2}\right\}. \quad (13)$$

Let us also consider the indicator function

$$\varphi(\mathbf{R}, t; \rho) = \delta(\rho(\mathbf{R}, t) - \rho), \quad (14)$$

which sifts $\rho(\mathbf{R}, t)$ at given ρ via the Dirac δ function. The total area of the regions, where ρ exceeds some threshold $\bar{\rho}$, is referred to as the cluster area, obtained as

$$S(t; \bar{\rho}) = \int d\mathbf{R}\,\theta(\rho(\mathbf{R}, t) - \bar{\rho}) = \int d\mathbf{R} \int_{\bar{\rho}}^\infty d\rho'\varphi(\mathbf{R}, t; \rho'), \quad (15)$$

where $\theta(\cdot)$ is the Heaviside (step) function. The total mass of the floating tracer within the cluster area is referred to as the cluster mass, obtained as

$$M(t; \bar{\rho}) = \int d\mathbf{R}\, \rho(\mathbf{R}, t)\theta(\rho(\mathbf{R}, t) - \bar{\rho})$$

$$= \int d\mathbf{R} \int_{\bar{\rho}}^{\infty} d\rho'\, \rho'\varphi(\mathbf{R}, t; \rho'). \qquad (16)$$

Ensemble averaging (15) and (16) yields

$$\langle S(t; \bar{\rho}) \rangle = \int d\mathbf{R} \int_{\bar{\rho}}^{\infty} d\rho'\, P(\mathbf{R}, t; \rho'), \qquad (17)$$

$$\langle M(t; \bar{\rho}) \rangle = \int d\mathbf{R} \int_{\bar{\rho}}^{\infty} d\rho'\, \rho' P(\mathbf{R}, t; \rho'), \qquad (18)$$

because the single-point PDF (11) is completely local, i.e., involves no lags in time and shifts in space. The ensemble averaging of the indicator function (14) yields

$$P(\mathbf{R}, t; \rho) = \langle \delta(\rho(\mathbf{R}, t) - \rho) \rangle \qquad (19)$$

and the expressions (17) and (18) become

$$\langle s_{\text{hom}}(t; \bar{\rho}) \rangle = \langle \theta(\rho(\mathbf{R}, t) - \bar{\rho}) \rangle = P\{\rho(\mathbf{R}, t) > \bar{\rho}\}$$

$$= \int_{\bar{\rho}}^{\infty} d\rho'\, P(t; \rho'),$$

$$\langle m_{\text{hom}}(t; \bar{\rho}) \rangle = \frac{1}{\rho_0} \int_{\bar{\rho}}^{\infty} d\rho'\, \rho' P(t; \rho'), \qquad (20)$$

where $s_{\text{hom}}(t; \bar{\rho})$ and $m_{\text{hom}}(t; \bar{\rho})$ are, respectively, the specific cluster area and specific cluster mass, defined by the threshold $\bar{\rho}$ [36,48]. Since $\rho(\mathbf{R}, t)$ is a positive-definite field, the clustering happens with probability one, and the corresponding limits

$$\lim_{t \to \infty} \langle s_{\text{hom}}(t; \bar{\rho}) \rangle \to 0, \quad \lim_{t \to \infty} \langle m_{\text{hom}}(t; \bar{\rho}) \rangle \to \frac{1}{\rho_0} \langle \rho(t) \rangle \quad (21)$$

assert that the cluster area shrinks to zero, while the cluster mass incorporates all the available tracer. From (11) and (20) one can derive the specific functions for the purely divergent velocity field

$$\langle s_{\text{hom}}(t, \bar{\rho}) \rangle = \text{Pr}\left(\frac{\ln(\rho_0 e^{-D^p t}/\bar{\rho})}{\sqrt{2D^p t}} \right),$$

$$\langle m_{\text{hom}}(t, \bar{\rho}) \rangle = \text{Pr}\left(\frac{\ln(\rho_0 e^{D^p t}/\bar{\rho})}{\sqrt{2D^p t}} \right), \qquad (22)$$

where ρ_0 is the initial density in the initial subdomain. At times much larger than the diffusion timescale τ, the following approximate estimates can be obtained from (22) and (13), by using the large-argument asymptotics of the probability integral [49]:

$$\langle s_{\text{hom}}(t, \bar{\rho}) \rangle = P\{\rho(\mathbf{R}, t) > \bar{\rho}\} \approx \sqrt{\frac{\rho_0}{\pi \bar{\rho} D^p t}} e^{-D^p t/4},$$

$$\langle m_{\text{hom}}(t, \bar{\rho}) \rangle / \rho_0 \approx 1 - \sqrt{\frac{\bar{\rho}}{\pi \rho_0 D^p t}} e^{-D^p t/4}. \qquad (23)$$

These relations describe the exponential clustering process, which happens with probability one. The single-point PDF, cluster area, and cluster mass conveniently describe this process, and together with their two-point extensions [36] they
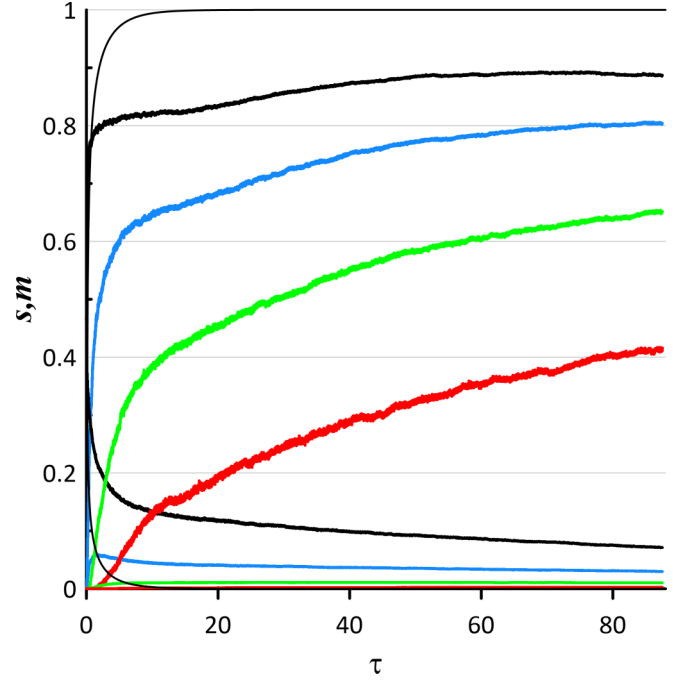

FIG. 5. Clustering area and mass for the purely nondivergent velocity regime ($\gamma = 0$) and for a single flow realization. The parameters are as in Fig. 4(c) and the curves correspond to $\bar{\rho} = 1$ (black), $\bar{\rho} = 2$ (blue), $\bar{\rho} = 4$ (green), and $\bar{\rho} = 8$ (red). The thin black curve corresponds to the asymptotic theory (22) and shows clearly the diffusion timescale.

are used further below for analysis of clustering in weakly divergent velocity fields.

We also employ the concept of a typical realization curve. Given a random process $z(t)$, this curve is defined as the median of the integral distribution function (12) and found as the solution $z^*(t)$ of the equation

$$\Phi(t; z^*(t)) = \int_0^{z^*(t)} dz'\, P(t; z') = \frac{1}{2}, \qquad (24)$$

which implies that for any time t, $P[z(t) > z^*(t)] = P[z(t) < z^*(t)] = \frac{1}{2}$. The typical realization curve of the distance between two particles [35] is

$$l^*(t) = \exp\left\{ \frac{1}{4}(D^s - D^p)t \right\}. \qquad (25)$$

When $D^s < D^p$, the average distance between the particles, as given by $l^*(t)$, attenuates exponentially, in accord with the exponential clustering process. When $D^s > D^p$, there is no exponential clustering, at least for the times such that the constraint

$$\frac{1}{4}D^s t \ll \ln \frac{l_{\text{corr}}}{l_0} \qquad (26)$$

holds [30], where l_0 is the average initial distance between the particles and l_{corr} is the spatial correlation radius of the velocity field (see Sec. III).

The statistical topography methodology offers a variety of useful characteristics such as the average contour length of the isoline corresponding to $\rho(\mathbf{R}, t) = \bar{\rho}$, which is estimated as

$$\langle L(t, \rho) \rangle = L_0 e^{D^s t}, \qquad (27)$$

where L_0 is its initial contour length [38,40]. In the purely nondivergent velocity field $L(t, \rho)$ grows exponentially
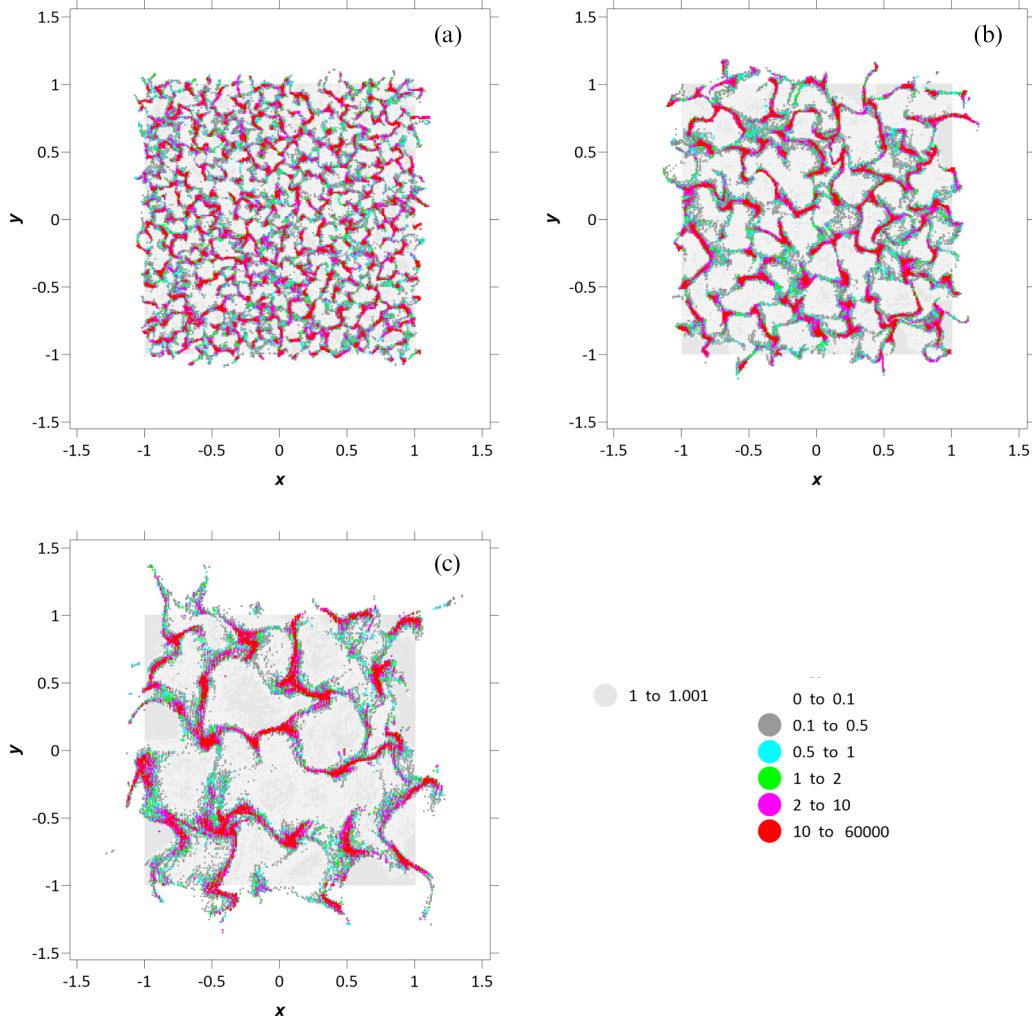
FIG. 6. Density distribution for $\gamma = 0.5$, $t = 4\tau$, and (a) $l = 0.04$ and $\sigma_U = 0.33$, (b) $l = 0.08$ and $\sigma_U = 0.67$, and (c) $l = 0.16$ and $\sigma_U = 0.67$. The rest is as in Fig. 1.

because the tracer patch is continuously stretched and fila-mented. We refer to this process as tracer fragmentation. In a weakly divergent velocity field, the tracer fragmentation affects and modulates the exponential clustering process; we address this issue later on.

III. KINEMATIC VELOCITY MODEL

In this section we introduce a kinematic model of random velocity field with prescribed correlation tensor and then study clustering in the model solutions.

A. Model formulation

Following [48,50–52], we use a spectral representation of the velocity field

$$U_\beta^p(\mathbf{R}, t) = \sigma_U \int d\mathbf{k}[a(k, t) + ib(k, t)]\frac{k_\beta}{k}\exp(i\mathbf{k} \cdot \mathbf{R}),$$

$$U_x^s(\mathbf{R}, t) = \sigma_U \int d\mathbf{k}[a(k, t) + ib(k, t)]\frac{k_y}{k}\exp(i\mathbf{k} \cdot \mathbf{R}),$$

$$U_y^s(\mathbf{R}, t) = -\sigma_U \int d\mathbf{k}[a(k, t) + ib(k, t)]\frac{k_x}{k}\exp(i\mathbf{k} \cdot \mathbf{R}),$$

$$\tag{28}$$

where σ_U is the standard deviation of the velocity, index β stands for either x or y, and $a(\mathbf{k}, t)$ and $b(\mathbf{k}, t)$ are random, Gaussian, δ-correlated-in-time spectral coefficients such that

$$\langle a(k, t) \rangle = \langle b(k, t) \rangle = \langle a(\mathbf{k}, t)b(\mathbf{k}', t') \rangle = 0,$$

$$\langle a(\mathbf{k}, t)a(\mathbf{k}', t') \rangle = \langle b(\mathbf{k}, t)b(\mathbf{k}', t') \rangle$$

$$= E(k)\delta(\mathbf{k} - \mathbf{k}')\delta(t - t'). \tag{29}$$

The velocity field (28) corresponds to the correlation tensor (4); in the physical space it is obtained by the inverse Fourier transform with random phase. The spectral density is

$$E(k, l) = \frac{1}{2\pi}\frac{l^4}{4}k^2\exp\left\{-\frac{1}{2}k^2l^2\right\} \tag{30}$$

and the velocity is characterized by the isotropic spatial corre-lation radius l_{corr}. The effective diffusivities (7) and (8) ensue from (30) and (3) by integration (7) and (8):

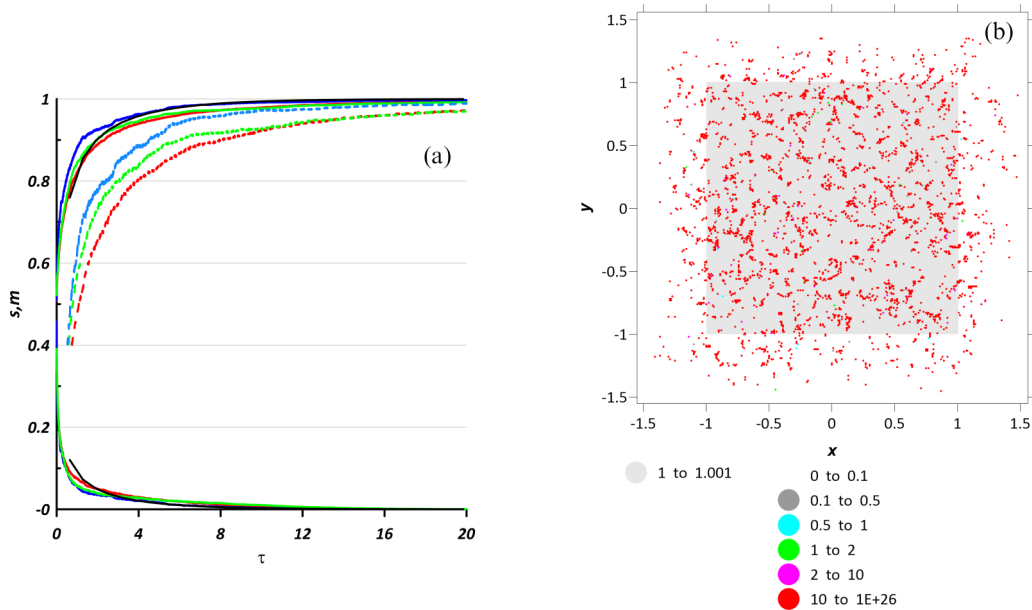$$D^s = (1 - \gamma)^2 D^0, \quad D^p = \gamma^2 D^0, \quad D^0 = \frac{\sigma_U^2}{l^2}t_0. \tag{31}$$

FIG. 7. Evolution of the clustering area and mass ($\bar{\rho} = 1$) for a single realization, $\gamma = 0.5$, and (a) $l = 0.04$ and $\sigma_U = 0.33$ (red curve), $l = 0.08$ and $\sigma_U = 0.67$ (green curve), and $l = 0.16$ and $\sigma_U = 0.67$ (blue curve). The black lines represent the asymptotics; the dashed lines correspond to the threshold value $\bar{\rho} = 4$. (b) Density distribution for $l = 0.04$, $\sigma_U = 0.33$, and time $t = 18\tau$. The other parameters are as in Fig. 6.

B. Numerical implementation

Given uniformly gridded velocity fields, Eqs. (1) and (2) are solved numerically along with a numerical simulation of the ensemble of advected Lagrangian particles [28,46,52–55]. Recall that we set $\kappa = 0$, so the governing equations are first-order linear PDEs that can be solved by the method of characteristics [28,46]. Evolution of each Lagrangian particle and its density and concentration are governed by

$$\frac{d\mathbf{R}}{dt} = \mathbf{U}(\mathbf{R}, t), \qquad \mathbf{R}(0) = \boldsymbol{\xi},$$

$$\frac{d\rho(t; \boldsymbol{\xi})}{dt} = -\frac{\partial \mathbf{U}(\mathbf{R}, t)}{\partial \mathbf{R}} \rho(t; \boldsymbol{\xi}), \qquad \rho(0; \boldsymbol{\xi}) = \rho_0(\boldsymbol{\xi}), \qquad (32)$$

$$\frac{dC(t; \boldsymbol{\xi})}{dt} = 0, \qquad C(0; \boldsymbol{\xi}) = C_0(\boldsymbol{\xi}),$$

where $\boldsymbol{\xi}$ is the initial position of the trajectory. These equations are integrated in time using the standard Euler-Itô scheme [56], and the Eulerian density and concentration fields are found on the trajectories

$$\rho(\mathbf{R}, t) = \rho(t) = \rho(t; \boldsymbol{\xi}(\mathbf{R}; t)),$$

$$C(\mathbf{R}, t) = C(t) = C(t; \boldsymbol{\xi}(\mathbf{R}; t)). \qquad (33)$$

In each grid cell within the initial tracer patch, we uniformly seed 900 Lagrangian particles and solve for them the governing equations. Since the framework is Lagrangian, the obtained fields are better resolved in the high-particle-density areas. Eventually, in the purely rotational velocity field, the number of particles becomes too small to resolve properly the fine structure of the tracer patch boundary (similar issues are discussed in [27,41,53,54]); in fact, since the boundary is known to become fractal, the number of particles for resolving

it tends to infinity. However, our main goal is to study the feasibility of clustering, not the associated fractal dimension.

We found that, in the immediate vicinity of clusters, in divergent velocity fields, a large number of particles with large density values aggregate; hence we argue that the exponential clustering is robustly captured and does not qualitatively depend on the threshold value $\bar{\rho}$. In the emerging areas with a low concentration of particles, the errors of the coarse-grained density estimates are high, but we focus not on the Lagrangian-particle density values but rather on the fact that in these areas these densities are clearly small. Moreover, we quantify the exponential clustering with the Monte Carlo approach and the integral cluster area and mass characteristics, which are independent of the structure and number of individual clusters: From $200 \times 200 \times 900 = 3.6 \times 10^7$ particles, more than 99% aggregate in clusters, which ensures the statistical confidence. Finally, we consider a finite tracer patch in an open domain. Also, we assume that the scales at which the exponential clustering occurs are much smaller than the scales at which the domain boundaries start playing an important role; therefore, the observed phenomenology is not affected by the boundary conditions.

IV. NUMERICAL RESULTS

In this section we focus on modeling the nondiffusive clustering in the implemented double-periodic domain ($|x| \leqslant 10$, $|y| \leqslant 10$) with the uniform numerical grid 2048^2. The initial uniform distribution of Lagrangian particles is in the subdomain ($|x| \leqslant 1$, $|y| \leqslant 1$), and there are 900 particles placed initially in each grid cell. Results for the strongly and weakly divergent velocity regimes are discussed and compared.

The random velocity field within each grid cell is treated as piecewise constant, which ensures that it has discontinuities
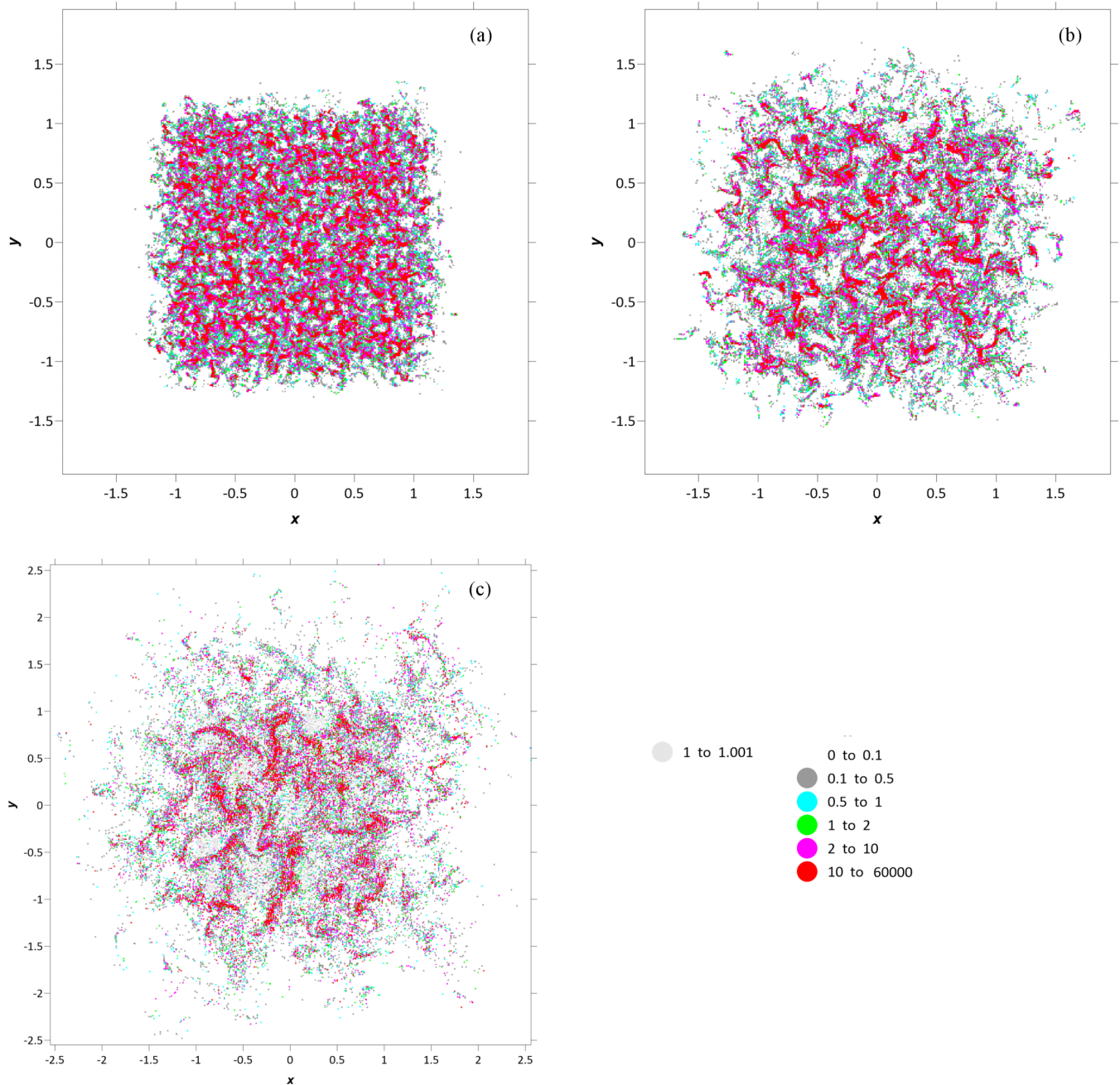
FIG. 8. Density distributions for $\gamma = 0.2$, $t = 25\tau$, and (a) $l = 0.04$ and $\sigma_U = 0.33$, (b) $l = 0.08$ and $\sigma_U = 0.67$, and (c) $l = 0.16$ and $\sigma_U = 1.33$. The other parameters are as in Fig. 6.

responsible for the white-noise stochastic process [48,52]. The coarse-grained tracer density and the normalized number, i.e., number in the bin divided by the bin area, of particles are found by averaging the corresponding Lagrangian statistics over finite-bin coarse-graining areas, and for the bin size we mostly use the numerical grid interval. Because each tracer conserves its mass, the corresponding cluster area experiences velocity divergence and scales as $\rho_0/\rho(t)$.

A. Purely divergent and nondivergent flow regimes

First, let us consider the limiting case of purely divergent velocity ($\gamma = 1$). The evolution of the particles is computed over the diffusion timescale $\tau = 1/D^p$ and for different values

of the spatial correlation radius l_{corr} (Figs. 1 and 2). Clustering is evident in the field of the normalized number of particles (Fig. 2), but it is much more pronounced in the density field (Fig. 1). Figure 3 shows that the clustering area and mass are very close to the asymptotic exponential prediction, even in individual realizations. We also find that the clustering depends weakly on the spatial correlation radius, provided the time is scaled diffusively, i.e., by τ.

Let us now compare clustering in the purely divergent ($\gamma = 1$) and nondivergent ($\gamma = 0$) velocity regimes (Figs. 4 and 5). In the latter regime there is almost no difference between clustering in the density field and in the field of the normalized number of particles, because the density is
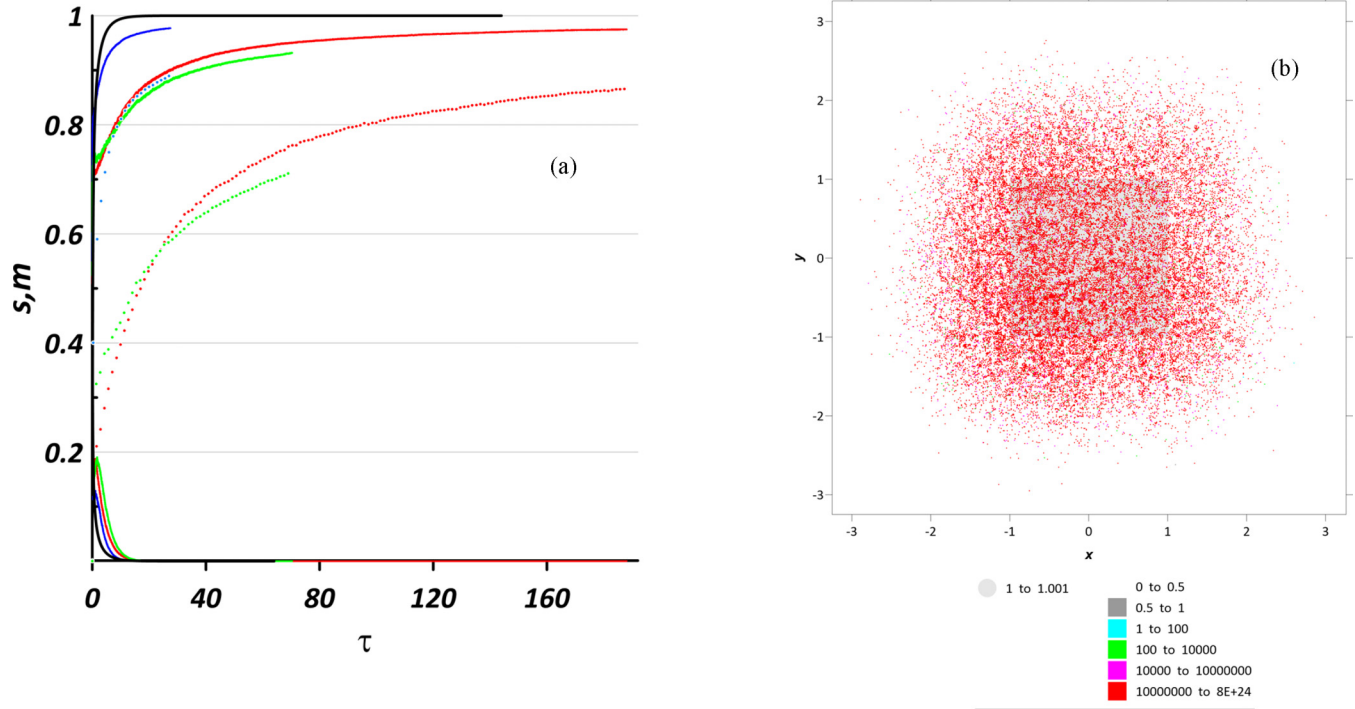
FIG. 9. Evolution of the clustering area and mass ($\bar{\rho} = 1$) for a single realization, $\gamma = 0.2$, and (a) $l = 0.04$ and $\sigma_U = 0.33$ (red curve), $l = 0.08$ and $\sigma_U = 0.67$ (green curve), and $l = 0.16$ and $\sigma_U = 0.67$ (blue curve). The black lines represent the asymptotics; the dashed lines correspond to the threshold value $\bar{\rho} = 4$. (b) Density distribution for $l = 0.04$ and $\sigma_U = 0.33$, and time $t = 18\tau$. The other parameters are as in Fig. 6.

materially conserved and particles do not aggregate. Furthermore, in this regime the asymptotic theory (25) predicts no exponential clustering at all. Instead, both fields are affected by stirring; as a result, they develop clusters due to the fragmentation process, which is fundamentally different from the exponential clustering. These clusters are transient and never statistically significantly aggregate density and particles, because this is just the chaotic stirring process.[1] As a result, the density excess over the threshold value is moderate: The number of grid cells with $\rho(\mathbf{R}, \tau) > 2$ is relatively small. Moreover, the maximum density value (about 5 after $t = 3\tau$) is significantly smaller than in the purely divergent case (where it is more than 100 at $t = \tau$). Strictly speaking, these high-density values do not signify exponential clustering in the sense of estimates (25) and (27), but reflect the fragmentation clustering. Figures 3 and 5 show the clustering area and mass based on $\bar{\rho} = 1$: The cluster mass decreases, but less so for large correlation radius ($l_{\text{corr}} = 0.16$), because of the slowed down fragmentation process. The clusters are typically small and uniformly distributed and there are no clusters on the scale of l_{corr}. We hypothesize that fragmentation clustering can dominate over exponential clustering in the presence of

_____

[1]We admit that the presence of dynamical constraints on the velocity field can significantly alter this type of clustering and lead to anomalously large values, provided the velocity field contains coherent structures, such as vortices and jets; investigating such scenarios is beyond the scope of the present paper.
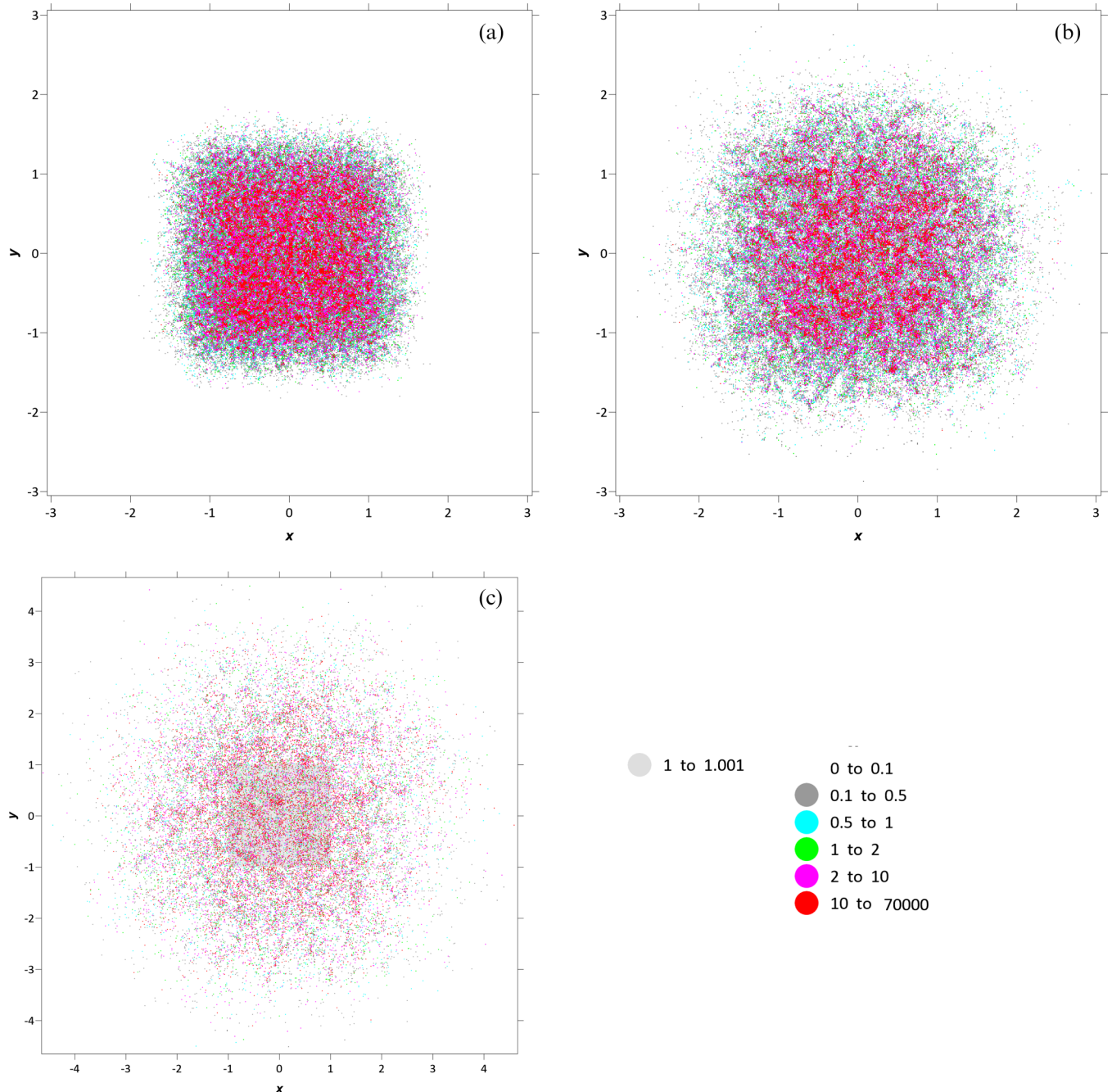
diffusion ($\kappa \neq 0$), but this analysis is beyond the scope of the paper.

B. Weakly divergent regime

Let us now consider a more realistic flow regime with equal contributions of the rotational and divergent components, $\gamma = 0.5$ (Fig. 6). The asymptotic estimate (25) still predicts no clustering; however, we found that the clustering not only occurs but is also very efficient. Overall, the clusters develop at a much slower rate (Fig. 7), relative to the purely divergent flow regime, but exponential clustering eventually dominates. The clustering slowdown takes place for all l_{corr} considered.

Let us now consider weakly divergent flow regimes with $\gamma = 0.2$ (Fig. 8) and also $\gamma = 0.1$, to illustrate the trends. Because of the strong rotational component, the particles are more quickly dispersed away from their initial positions, and hence we have to increase the model domain. Although the asymptotic theory predicts no exponential clustering, we find that it still takes place, but with a significantly slower rate. Figure 9(a) shows that initial clustering is faster due to the fragmentation process, but then it slows down, so the exponential clustering behavior is reached at about $t = 25\tau$. Stirring induced by the rotational velocity component is significant, and in accord with this we have $D^s \approx 16D^p$; concurrently, the clustering process evolves over the rotational diffusion timescale D^s, which is much longer (Fig. 9). Clusters on the scale l_{corr} do not emerge due to the shearing effect of the rotational component, which accelerates fragmentation of the clusters. Exponential clustering still occurs, even for

FIG. 10. Density distributions for $\gamma = 0.1$, $t = 25\tau$, and (a) $l = 0.04$ and $\sigma_U = 0.33$, (b) $l = 0.08$ and $\sigma_U = 0.67$, and (c) $l = 0.16$ and $\sigma_U = 1.33$. The other parameters are as in Fig. 6.

$\gamma = 0.1$ (Figs. 10 and 11), but with progressively slower rates. The dependence on l_{corr} is similar to the $\gamma = 0.2$ regime, as manifested by the cluster area and mass curves.

Let us now discuss the effects of coarse graining on the fields of interest. If it is too coarse, it may appear that all particles within the averaging-bin region are clustered while the corresponding cluster mass is underpredicted (see Fig. 9, where the clusters are red). To explain this, let us consider in detail the regime $\gamma = 0.2$ and refine its spatial averaging by 100 times in each spatial direction (Fig. 12): The fine structure of clusters, otherwise smeared out by the coarse graining, becomes apparent. Hence, within each

coarse-grained cluster there are in fact many finer-scale clusters revealed, even for a relatively long time. To summarize, some caution is required to interpret coarse-grained fields, and in this regard statistical topography diagnostics are robust and useful.

V. CONCLUSION

This study has dealt with clustering, i.e., localized aggregation, of floating tracers and material objects, such as plastic, microplastic, oil spills, and sargassum, at the ocean surface. The main motivation was to address at the fundamental level
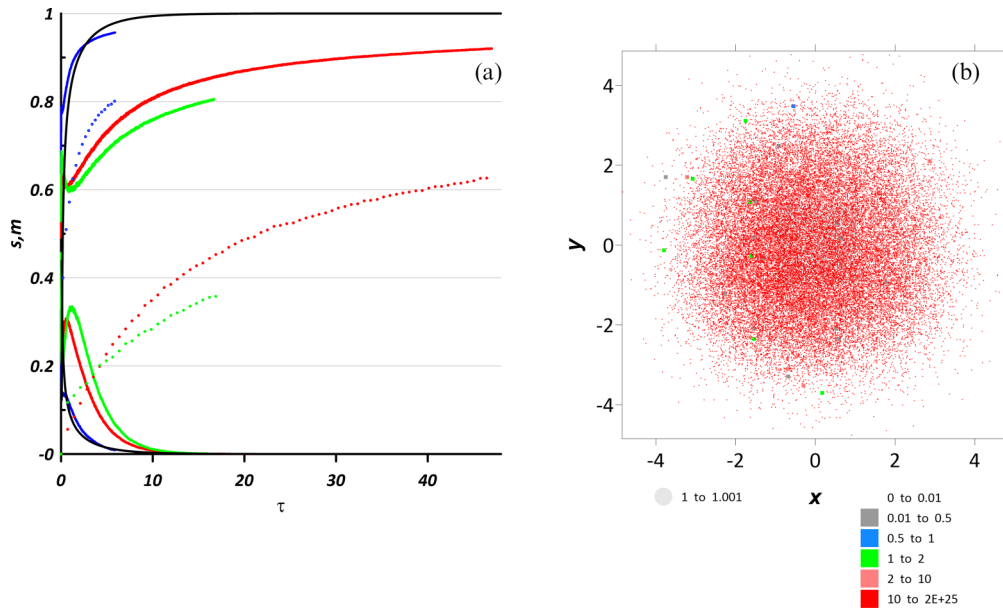
FIG. 11. Evolution of the clustering area and mass ($\bar{\rho} = 1$) for a single realization, $\gamma = 0.1$, and (a) $l = 0.04$ and $\sigma_U = 0.33$ (red curve), $l = 0.08$ and $\sigma_U = 0.67$ (green curve), and $l = 0.16$ and $\sigma_U = 0.67$ (blue curve). The black lines represent the asymptotics; the dashed lines correspond to the threshold value $\bar{\rho} = 4$. (b) Density distribution for $l = 0.04$ and $\sigma_U = 0.33$, and time $t = 18\tau$. The other parameters are as in Fig. 6.
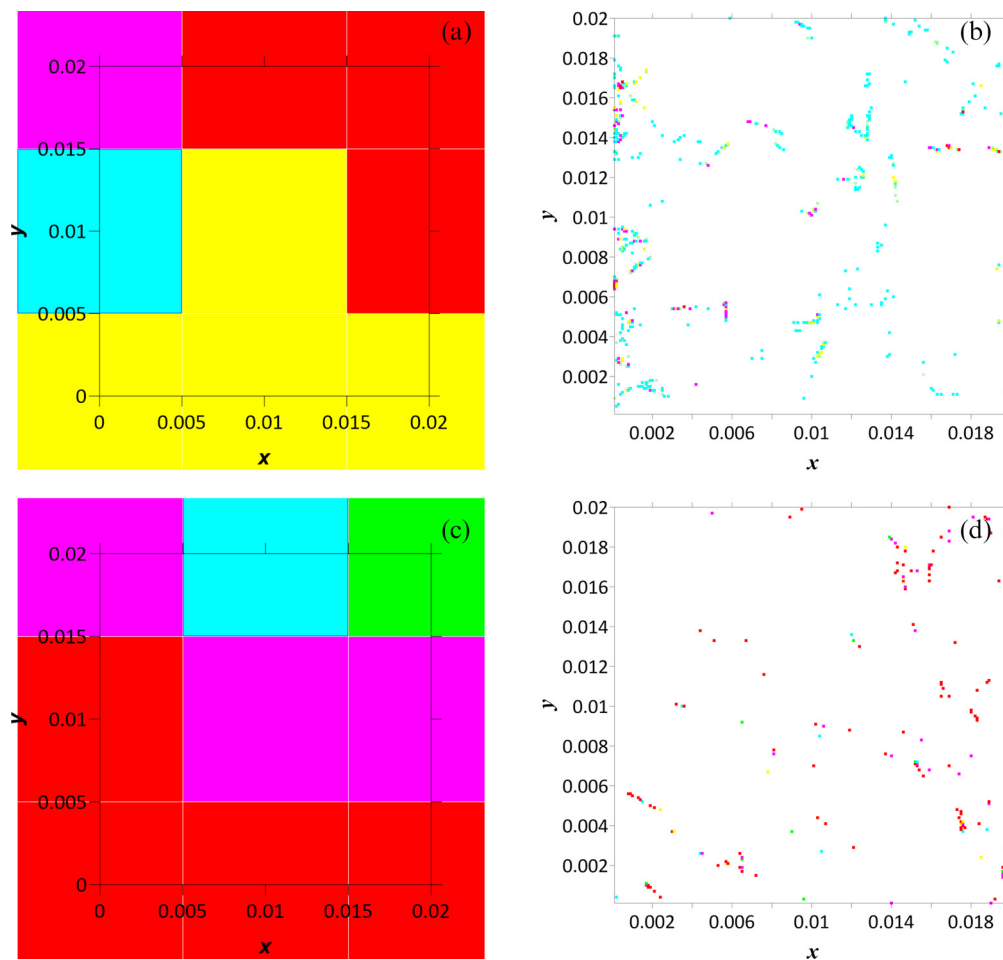

FIG. 12. Effect of coarse graining on the fields of the normalized number of particles, shown here for $\gamma = 0.2$, $l = 0.04$, $\sigma_U = 0.33$, and (a) and (b) $t = 0.422\tau$ and (c) and (d) $t = 2.322\tau$: (a) and (c) close-up of the subdomain from Fig. 8 and (b) and (d) same as (a) and (c) but with 100 times finer coarse-graining resolution.

growing environmental concerns on the adverse effects of floating pollution on marine life.

As a starting point, we noted that passive and floating, i.e., buoyant, tracers evolve in fundamentally different ways, because the passive-tracer concentration is materially conserved, i.e., remains constant on the Lagrangian particles, whereas the floating-tracer density (we use this term to distinguish it from the passive-tracer concentration) changes on the Lagrangian particles due to the compressibility effect induced by the surface flow divergence; we referred to these processes as C and D clustering, respectively. Another characteristic is the normalized number of particles per unit area, which can also experience different types of clustering; we refer to this process as L clustering. Our main focus was on the D clustering, but some comparisons with L clustering were made for clarity, to show that these processes have profoundly different characteristics. The C clustering can form only as part of the fragmentation clustering process, which is due to nonuniform flow advection of the initially inhomogeneous distribution of concentration; in general, this is just an aspect of chaotic stirring. For the D and L clustering, in addition to the fragmentation process, there is also exponential clustering, which is the main subject of this paper. The process is characterized by emergence of a set of localized (and eventually singular) clusters with ever-shrinking area that eventually collects all the available tracer.

We represented the tracer by ensembles of Lagrangian particles and considered their evolution in random kinematic velocity fields. The goal was to establish and interpret the clustering properties, as induced by 2D velocity fields consisting of divergent (potential) and rotational (nondivergent) flow components, which represent the geostrophic and ageostrophic parts of mesoscale eddy field. For divergent velocity fields, the existing asymptotic theories [29,35,41–43] predict exponential-in-time clustering, which depends on the velocity correlation length scale. Estimates of the fractal dimension associated with the asymptotic clustering were obtained in Refs. [31,41–43]. All these theories predict asymptotic states and do not describe the transition to these states at finite times. In this paper we studied the clustering process at finite times, in weakly divergent velocity fields, and by means of the statistical topography methodology.

We demonstrated that, despite the asymptotic predictions that exponential clustering occurs only for velocity fields with the divergent component larger than the rotational one, the exponential clustering is still feasible for weakly divergent velocity fields. However, the rate of clustering is significantly slowed down, because it becomes controlled by the rotational flow component and its associated diffusion timescale. We also found that in weakly divergent flow regimes, there is also fragmentation clustering, which is due to chaotic stirring of inhomogeneous tracer distributions by inhomogeneous advection that depends on the velocity correlation length scale.

Future research extensions based on the presented results may consider additional effects of large-scale flows, explicit eddy diffusion, the finite lifetime of a tracer, and inertial effects due to the buoyancy and finite size of floating objects. Including finite time correlations in the kinematic flow model

and considering dynamically constrained and progressively more realistic flows are also obvious avenues for new advances on the clustering problem.

APPENDIX

Given the acting 3D velocity field $\mathbf{u} = (u, v, w)$, the continuity equation for the passive-tracer concentration $C_{3D}(x, y, z, t)$ is

$$\frac{\partial C_{3D}}{\partial t} + \frac{\partial (u C_{3D})}{\partial x} + \frac{\partial (v C_{3D})}{\partial y} + \frac{\partial (w C_{3D})}{\partial z} = 0.$$

Let us restrict our dynamical description to the 2D surface of the ocean and assume the rigid-lid approximation $w(x, y, 0, t) = 0$, with the surface velocity expressed as $\mathbf{U} = (U, V)$. In this case, the 2D governing equation for the surface concentration $C(x, y, t) = C_{3D}(x, y, 0, t)$ can be written as

$$\frac{\partial C}{\partial t} + \mathbf{U} \cdot \boldsymbol{\nabla} C + C \boldsymbol{\nabla} \cdot \mathbf{U} + C \frac{\partial w}{\partial z}\bigg|_{z=0} = 0.$$

Now let us invoke the incompressible fluid density continuity equation $\boldsymbol{\nabla} \cdot \mathbf{u} = 0$ and express

$$\frac{\partial w}{\partial z}\bigg|_{z=0} = -\boldsymbol{\nabla} \cdot \mathbf{U}.$$

By taking this into account, the governing equation for the evolution of the passive-tracer concentration on the ocean surface becomes

$$\frac{\partial C}{\partial t} + \mathbf{U} \cdot \boldsymbol{\nabla} C = 0.$$

Now let us derive a similar equation for the floating-tracer density ρ by writing the standard continuity equation

$$\left(\frac{\partial}{\partial t} + \frac{\partial}{\partial \mathbf{r}} \right) \mathbf{u}(\mathbf{r}, t) \rho(\mathbf{r}, t) = 0.$$

Let the floating tracer density be in the form $\rho(\mathbf{r}, t) = \rho(\mathbf{R}, t)\delta(z)$, where $\delta(z)$ is the Dirac delta. The equation means that all the density is constrained at the surface $z = 0$. In

addition, $\mathbf{u}(\mathbf{r}) = (\mathbf{U}(\mathbf{r}), w(\mathbf{r}))$ and $\mathbf{r} = (\mathbf{R}, z)$, and thus

$$\left(\frac{\partial}{\partial t} + \frac{\partial}{\partial \mathbf{r}}\right)\mathbf{u}(\mathbf{r}, t)\rho(\mathbf{R}, t)\delta(z) = 0.$$

Scalar multiplying yields

$$\delta(z)\left(\frac{\partial}{\partial t} + \frac{\partial}{\partial \mathbf{R}}\right)\mathbf{U}(\mathbf{r}, t)\rho(\mathbf{R}, t)$$

$$+ \delta(z)\left(\frac{\partial}{\partial t}\right)w(\mathbf{r}, t)\rho(\mathbf{R}, t)$$

$$+ \delta(z)\frac{\partial}{\partial z}w(\mathbf{r}, t)\rho(\mathbf{R}, t)$$

$$+ w(\mathbf{r}, t)\rho(\mathbf{R}, t)\frac{\partial}{\partial z}\delta(z) = 0. \tag{A1}$$

Integrating over z and taking into account the δ-function property, one obtains

$$\left(\frac{\partial}{\partial t} + \frac{\partial}{\partial \mathbf{R}}\right)\mathbf{U}(\mathbf{r}, t)\rho(\mathbf{R}, t)$$

$$+ \left(\frac{\partial}{\partial t}\right)w(\mathbf{R}, 0, t)\rho(\mathbf{R}, t)$$

$$+ \rho(\mathbf{R}, t)\frac{\partial}{\partial z}w(\mathbf{R}, 0, t)$$

$$- \rho(\mathbf{R}, t)\frac{\partial}{\partial z}w(\mathbf{R}, 0, t) = 0. \tag{A2}$$

With $w(\mathbf{R}, 0, t) = 0$, one arrives at

$$\frac{\partial \rho(\mathbf{R}, t)}{\partial t} + \mathbf{U}(\mathbf{r}, t) \cdot \nabla\rho(\mathbf{R}, t) + \rho(\mathbf{R}, t)\nabla \cdot \mathbf{U}(\mathbf{r}, t) = 0.$$

Note that the last term, which represents density compression by converging velocity, does not have its counterpart in the governing equation for C.

---

[1] A. Okubo, *Diffusion and Ecological Problems: Mathematical Models*, Biomathematics (Springer, Berlin, 1980), Vol. 10, p. 254.

[2] W. D. McComb, *The Physics of Fluid Turbulence*, Oxford Engineering Science Series Vol. 25 (Clarendon, Oxford, 1990).

[3] J. A. Jacobs, H. S. Huntley, A. D. Kirwan, B. L. Lipphardt, T. Campbell, T. Smith, K. Edwards, and B. Bartes, J. Geophys. Res.: Oceans **121**, 180 (2016).

[4] A. Kostinski and R. Shaw, J. Fluid Mech. **434**, 389 (2001).

[5] G. Dagan, Annu. Rev. Fluid Mech. **19**, 183 (1987).

[6] I. de Pater and J. Lissauer, *Planetary Science* (Cambridge University Press, Cambridge, 2001).

[7] S. F. Shandarin and Y. B. Zeldovich, Rev. Mod. Phys. **61**, 185 (1989).

[8] K. L. Law, S. Moret-Ferguson, N. A. Maximenko, G. Proskurowski, E. E. Peacock, J. Hafner, and C. M. Reddy, Science **329**, 1185 (2010).

[9] A. Cozar, F. Echevarria, J. I. Gonzalez-Gordillo, X. Irigoien, B. Ubeda, S. Hernandez-Leon, A. T. Palma, S. Navarro, J. G. de Lomas, A. Ruiz, M. L. F. de Puelles, and C. M. Duarte, Proc. Natl. Acad. Sci. USA **111**, 10239 (2014).

[10] B. Eckhardt and J. Schumacher, Phys. Rev. E **64**, 016314 (2001).

[11] J. Schumacher and B. Eckhardt, Phys. Rev. E **66**, 017303 (2002).

[12] L. Thomas, A. Tandon, and A. Mahadevan, *Submesoscale Processes and Dynamic* (American Geophysical Union, Washington, DC, 2008), pp. 17–38.

[13] S. Karimova, Adv. Space Res. **50**, 1107 (2012).

[14] G. Dencausse, R. Morrow, M. Rog, and S. Fleury, Ocean Dynam. **64**, 61 (2014).

[15] J. Kalda, T. Soomere, and A. Giudici, J. Mar. Syst. **129**, 56 (2014).

[16] A. C. Haza, T. M. Özgökmen, and P. Hogan, Ocean Model. **107**, 28 (2016).

[17] P. Gaube and D. J. McGillicuddy, Jr., Deep-Sea Res. Pt. I **122**, 1 (2017).

[18] G. Väli, V. M. Zhurbas, J. Laanemets, and U. Lips, Fund. Prikl. Gidrofiz. **11**, 21 (2018).

[19] E. A. D'Asaro, A. Y. Shcherbina, J. M. Klymak, J. Molemaker, G. Novelli, C. M. Guigand, A. C. Haza, B. K. Haus, E. H. Ryan, G. A. Jacobs, H. S. Huntley, N. J. M. Laxague, S. Chen, F. Judt, J. C. McWilliams, R. Barkan, A. D. Kirwan, Jr., A. C. Poje, and T. M. Özgökmen, Proc. Natl. Acad. Sci. USA **115**, 1162 (2018).

[20] G. M. Reznik and R. Grimshaw, J. Fluid Mech. **443**, 351 (2001).

[21] E. Pallàs-Sanz and A. Viùdez, J. Phys. Oceanogr. **37**, 84 (2007).

[22] V. V. Zhmur, *Mezoscale Ocean Eddies* (GEOS, Moscow, 2011).

[23] P. Wang, J. C. McWilliams, and Z. Kizner, J. Fluid Mech. **712**, 327 (2012).

[24] J. C. McWilliams, Proc. R. Soc. A **472**, 20160117 (2016).

[25] Z. Zhang and B. Qiu, Geophys. Res. Lett. **45**, 11847 (2018).

[26] M. Maxey, J. Fluid Mech. **174**, 441 (1987).

[27] G. Boffetta, J. Davoudi, B. Eckhardt, and J. Schumacher, Phys. Rev. Lett. **93**, 134501 (2004).

[28] V. I. Klyatskin, Phys. Usp. **37**, 501 (1994).

[29] V. I. Klyatskin and A. I. Saichev, JETP **84**, 716 (1997).

[30] V. I. Klyatskin, Phys. Usp. **46**, 667 (2003).

[31] J. R. Cressman and W. I. Goldburg, J. Stat. Phys. **113**, 875 (2003).

[32] V. I. Klyatskin, JETP **99**, 1005 (2004).

[33] R. Monchaux, M. Bourgoin, and A. Cartellier, Phys. Fluids **22**, 103304 (2010).

[34] M. Bourgoin and H. Xu, New J. Phys. **16**, 085010 (2014).

[35] V. I. Klyatskin, *Stochastic Equations: Theory and Applications in Acoustics, Hydrodynamics, Magnetohydrodynamics, and Radiophysics* (Springer, Cham, 2015), Vols. 1 and 2.

[36] V. I. Klyatskin, Phys. Usp. **59**, 67 (2016).

[37] P. Gutierrez and S. Aumaitre, Eur. J. Mech. B: Fluids **60**, 24 (2016).

[38] V. I. Klyatskin, W. A. Woyczynski, and D. Gurarie, in *Stochastic Modelling in Physical Oceanography*, edited by R. Adler, P. Müller, and B. L. Razovsky, Progress in Probability (Birkhäuser, Boston, 1996), Vol. 39, pp. 221–269.

[39] V. Klyatskin, W. Woyczynski, and D. Gurarie, J. Stat. Phys. **84**, 797 (1996).

[40] A. Saichev and W. Woyczynski, in *Stochastic Models in Geosystems*, edited by S. Molchanov and W. Woyczynski, IMA Volumes in Mathematics and its Applications (Springer, New York, 1996), Vol. 85, pp. 359–400.

[41] G. Falkovich, K. Gawedzki, and M. Vergassola, Rev. Mod. Phys. **73**, 913 (2001).

[42] J. Bec, K. Gawedzki, and P. Horvai, Phys. Rev. Lett. **92**, 224501 (2004).

[43] I. Fouxon, Phys. Rev. Lett. **108**, 134502 (2012).

[44] E. Ryzhov, K. Koshel, and D. Stepanov, Theor. Comput. Fluid Dyn. **24**, 59 (2010).

[45] K. V. Koshel and S. V. Prants, Phys. Usp. **49**, 1151 (2006).

[46] K. V. Koshel, E. A. Ryzhov, and V. V. Zhmur, Phys. Rev. E **92**, 053021 (2015).

[47] K. V. Koshel, E. A. Ryzhov, and X. J. Carton, Fluids **4**, 14 (2019).

[48] V. I. Klyatskin and K. V. Koshel, Phys. Rev. E **95**, 013109 (2017).

[49] *NIST Handbook of Mathematical Functions*, edited by F. W. J. Olver, D. W. Lozier, R. F. Boisvert, and C. W. Clark (Cambridge University Press, Cambridge, 2010).

[50] A. P. Roberts and M. Teubner, Phys. Rev. E **51**, 4141 (1995).

[51] C. L. Zirbel and E. Cinlar, in *Stochastic Models in Geosystems* (Ref. [40]), p. 459.

[52] K. V. Koshel and O. V. Alexandrova, Izv. Atmos. Ocean. Phys. **35**, 578 (1999).

[53] O. Gat, I. Procaccia, and R. Zeitak, Phys. Rev. Lett. **80**, 5536 (1998).

[54] U. Frisch, A. Mazzino, and M. Vergassola, Phys. Rev. Lett. **80**, 5532 (1998).

[55] K. V. Koshel, E. A. Ryzhov, and V. V. Zhmur, Nonlin. Process. Geophys. **20**, 437 (2013).

[56] P. Kloeden and E. Platen, *Numerical Solution of Stochastic Differential Equations* (Springer, Berlin, 1992).